JOURNAL OF MATERIALS SCIENCE 11 (1976) 264–272

Deformation in spinel

T. E. MITCHELL, L. HWANG, A. H. HEUER
Department of Metallurgy and Materials Science, Case Western Reserve University, Cleveland, Ohio, USA

Stoichiometric $MgAl_2O_4$ spinel was deformed in compression at temperatures from 1790 to 1895° C and the dislocation structures analysed by transmission electron microscopy. $\{1\,1\,1\}\langle 1\,1\,0\rangle$ slip was observed on both the primary and cross-slip systems, and there was much secondary slip as well; all six $\langle 1\,1\,0\rangle$ Burgers vectors were present in electron micrographs. This secondary slip leads to very high work-hardening rates, approximately $\mu/70$ at 1790° C, where μ is the shear modulus. Since it is known that deformation in non-stoichiometric (alumina-rich) spinel crystals occurs by $\{1\,1\,0\}\langle 1\,1\,0\rangle$ slip, the electrostatic and geometric aspects of $\frac{1}{4}\langle 1\,1\,0\rangle$ dislocations moving on $\{1\,1\,1\}$ and $\{1\,1\,0\}$ planes are considered in some detail. It is porposed that the octahedral cation vacancies present in non-stoichiometric spinel diffuse to dislocations during deformation and thus favour $\{1\,1\,0\}$ slip.

1. Introduction

Deformation in spinel has been of interest since Hornstra predicted [1] that slip should occur on $\{1\,1\,1\}\langle 1\,1\,0\rangle$, the same family of slip systems exhibited by the ductile f c c metals. Stoichiometric spinel is quite strong, however. The present authors have shown [2] that the yield stress at 1800° C in stoichiometric crystals is such that only sapphire oriented to suppress both basal and prismatic slip is stronger. The high strength of stoichiometric crystals was attributed to a large Peierls force; the lower strengths of non-stoichiometric (alumina-rich) crystals was attributed to cation vacancies, which are necessarily present in crystals with the Al_2O_3:MgO ratio, n, >1. In the earlier work [2], $\{1\,1\,1\}$ slip in stoichiometric $MgAl_2O_4$ was established unambiguously and the transition from $\{1\,1\,1\}$ to $\{1\,1\,0\}$ slip as n increased above 1 was explained in terms of a lowering of the Peierls barrier for $\{1\,1\,0\}$ slip by the cation vacancies. In this paper, we discuss the dislocation structures in stoichiometric crystals deformed in the temperature range 1790 to 1895° C in more detail and present further discussion on the transition from $\{1\,1\,1\}$ to $\{1\,1\,0\}$ slip with increasing cation vacancy content. Before presenting the experimental data, however, crystal chemical and crystallographic aspects of the structure as it pertains to the Burgers vectors of both perfect and dissociated dislocations will be presented.

The close-packed oxygen framework in spinel is in almost perfect f c c packing. In the stoichiometric crystals, one half of the octahedral and one eighth of the tetrahedral interstices are occupied by the cations. An early neutron diffraction study [3] suggested that spinel was nearly normal, i.e. that most the tetrahedral sites were occupied by the divalent Mg ions. Later work [4] has shown that the degree of inversion is variable (10 to 15%) and appears to depend on thermal history. It is likely from entropic considerations that at the high temperatures needed for deformation studies, crystals have a random arrangement of cations, i.e. $\frac{1}{3}$ of the tetrahedral sites are occupied by Mg, as occurs in $MgFe_2O_4$ at high temperatures [5]. Jagodinski and Saalfield [6] have shown that the vacancies in non-stoichiometric crystals are predominantly on the octahedral sites.

It is agreed [2, 7–10] that the Burgers vector for dislocations in spinel is $a_0/2\langle 1\,1\,0\rangle$, the shortest lattice vector and twice the anion–anion spacing (a_0 is the lattice parameter). Dislocation dissociation into two colinear half-partials

$$a_0/2\langle 1\,1\,0\rangle \rightarrow a_0/4\langle 1\,1\,0\rangle + a_0/4\langle 1\,1\,0\rangle \quad (1)$$

has been observed [7–10], as predicted [1]. Since

$a_0/4\langle 1\,1\,0\rangle$ is the anion–anion distance, the stacking fault caused by such dissociation only involves a stacking error in the cation lattice. The further dissociation into quarter partials predicted by Hornstra [1]

$$a_0/4\langle 1\,1\,0\rangle \rightarrow a_0/12\langle 1\,2\,1\rangle + a_0/12\langle 2\,1\,\bar{1}\rangle \quad (2)$$

has not been observed, even with the high resolution (~20 Å) possible with weak beam electron microscopy [8–10]. The lack of visible dissociation into quarter partials is due to the high stacking fault energy associated with the fault generated by Equation 2, which involves errors in both the cation and anion sublattices, although Reaction 2 may accurately describe the core structure of an $a_0/4\langle 1\,1\,0\rangle$ dislocation. Reaction 2 is not possible when slip occurs on $\{1\,1\,0\}$, the observed slip plane for non-stoichiometric crystals [7].

2. Results

2.1. Mechanical properties

Shear stress–shear strain curves for stoichiometric spinel crystals deformed in compression at temperatures between 1790 and 1895° C are illustrated in Fig. 1. (Detailed experimental techniques are given in [2]). The compression axis is also given in the figure and is oriented near the centre of the stereographic triangle such as to be 45° from (1 1 1) and $[\bar{1}\,0\,1]$. Shear stresses and shear strains were calculated on the assumption of $(1\,1\,1)[\bar{1}\,0\,1]$ slip. Surface traces corresponding to the (1 1 1) primary slip planes were in fact observed by optical microscopy and dislocations with $\frac{1}{2}[\bar{1}\,0\,1]$ Burgers vectors were analysed by transmission electron microscopy, as reported previously [2]. However, slip traces parallel to the $(1\,\bar{1}\,1)$ cross-slip plane were equally prominent, in spite of the low Schmid factor on this plane. This is believed to be due to the lower normal stress acting on the cross-slip plane compared to the primary slip plane.

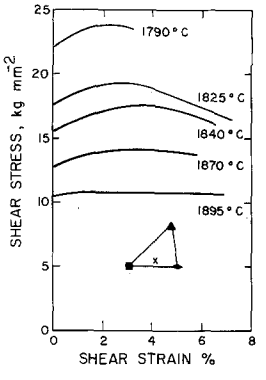

Figure 1 Curves of shear stress (σ) versus shear strain (ϵ) for stoichiometric spinel crystals deformed in compression. Strain-rate $\dot{\epsilon} = 1.4 \times 10^{-4}\,\mathrm{sec}^{-1}$.

Fig. 1 shows that both the yield stress and the work-hardening behaviour are strongly temperature dependent. The initial work-hardening rate varies from $\sim \mu/70$ (where μ is the shear modulus) at 1790° C to near zero at 1895° C. In addition, the work-hardening rate decreases with increasing strain and, in the lower temperature range, there is a prominent maximum in the stress–strain curve at ~3%, after which work-softening sets in. This latter aspect of slip in spinel is not understood at present and will be the subject of further investigation.

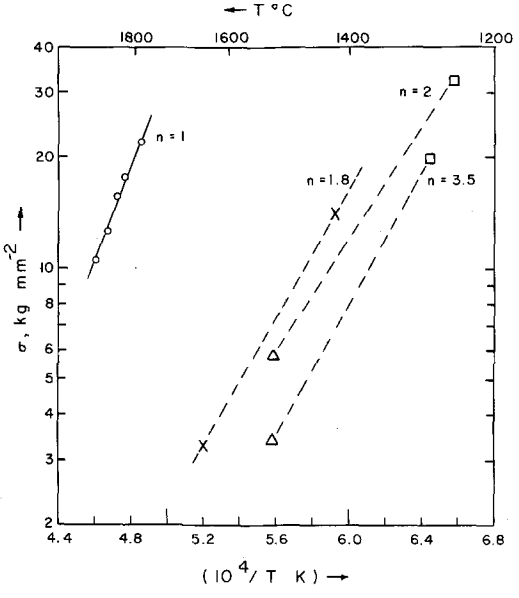

Figure 2 Logarithm of the resolved yield stress (σ) versus reciprocal temperature for various values of n (Al_2O_3: MgO ratio) from 1 to 3.5: $n = 1$ from present study, $n = 2$ and 3.5 from Lewis [7] and Radford and Newey [11], $n = 1.8$ extrapolated from creep data of Doukhan *et al.* [9]. Strain-rate $\dot{\epsilon} \simeq 10^{-4}\,\mathrm{sec}^{-1}$.

The logarithm of the yield stress is plotted against reciprocal temperature in Fig. 2. The straight line indicates that the relationship between stress (σ), temperature (T) and strain-rate ($\dot{\epsilon}$) can be expressed as:

$$\dot{\epsilon} = A\sigma^y \exp(-\Delta H/RT) \quad (3)$$

$$\text{i.e.} \quad \sigma = (\dot{\epsilon}/A)^{1/y} \exp(\Delta H/yRT) \quad (4)$$

where A and y are constants and ΔH is an activation enthalpy. For comparison, Fig. 2 also gives values of the yield stress of non-stoichiometric

spinel determined by Lewis [7] for $n = 2$ and $n = 3.5$ crystals, and by Radford and Newey [11] for $n = 2$ and $n = 3$ crystals. The dashed line has been extrapolated from the creep data of Doukhan *et al.* [9] for $n = 1.8$ samples, which gave a good fit to Equation 3 with $y = 3.9$ and $\Delta H = 5.3\,\text{eV}$ (stresses for constant strain-rate tests were estimated from Equation 4 using $\dot{\epsilon} \cong 1 \times 10^{-4}\,\text{sec}^{-1}$). At a given temperature, the non-stoichiometric crystals are seen to yield at stresses an order of magnitude lower than the stoichiometric crystals. Correspondingly, the brittle-to-ductile temperature is also much lower ($\sim 1250^\circ$ C [7] versus $\sim 1680^\circ$ C [2]). Values of the parameter y were not determined in the present investigation. However, if y is assumed to have the value 3.9, as determined by Doukhan *et al.* [9], then the slope of the line in Fig. 2 for stoichiometric crystals yields an activation energy $\Delta H \cong 9.0\,\text{eV}$, as compared with $\Delta H \cong 5.3\,\text{eV}$ for non-stoichiometric crystals. Since Equation 3 is a dislocation climb equation, the activation energy should correspond to that for self-diffusion and the lower value for non-stoichiometric spinel could be interpreted as due to the existence of cation vacancies in the structure. However, Ando and Oishi [12] have recently determined self-diffusion coefficients for oxygen (shown to be the slowest moving species in spinel and hence probably rate-controlling) for crystals with values of n from 1.0 to 2.2 and found $\Delta H = 4.55 \pm 0.26\,\text{eV}$. ΔH was independent of n and D for the $n = 2.2$ crystal was only $\sim 25\%$ higher than that for the $n = 1$ crystal. Using this value of ΔH, the slope of Fig. 2 yields a y value of ~ 2. It is possible, however, that yielding and steady state creep cannot be related through Equation 3 or 4 because the Peierls force is much more important in the yielding than in the creep behaviour.

2.2. Dislocation substructures

Dislocation substructures were determined by transmission electron microscopy of thin foils prepared from stoichiometric crystals deformed at $\sim 1800^\circ$ C (Fig. 3). The substructure was observed to be remarkably variable and typical dislocation arrangements in one particular thin foil cut parallel to the (1 1 1) primary slip plane are shown in Fig. 3a to d. The relatively uniform dislocation network structure seen in Fig. 3a, which have a tendency towards a hexagonal character, is the most characteristic. The loops and curved dislocation arrangement in Fig. 3b is also quite frequently observed. The arrangement in Fig. 3c is less common, and consists of long parallel edge dislocations which have appreciable internal stresses around them, as deduced by the surrounding extinction contours. However, relatively few dislocations appeared to be confined to the primary slip plane, as illustrated in Fig. 3d, which shows an area containing many inclined secondary dislocations. The hexagonal dislocation networks were found by stereomicroscopy to lie on planes randomly oriented in the crystal. Because of the strong cross-slip lines observed on the surface, foils were also cut parallel to this plane. As seen in Fig. 3e, dislocation arrangements in the cross-slip plane look much the same as those in the primary slip plane and consist of randomly oriented hexagonal networks. Foils cut parallel to other planes show the same type of dislocation arrangement; Fig. 3f shows an area of a (1 0 1) foil containing both networks and long primary edge dislocations which are out of contrast. The fact that dislocations were rarely observed to lie in well-defined slip planes may be explained by the high deformation temperatures, which enable dislocations to climb rapidly into lower energy network configurations. Long parallel edge dislocations were only observed in small number in the primary slip plane; these probably resulted from the last slip just prior to the termination of the compression test, and before the dislocations had time to climb into networks.

Diffraction contrast analysis showed that Burgers vectors were all of the type $a_0/2\langle 1\,1\,0\rangle$, with all six vectors represented. The nodes in the hexagonal networks were found to correspond to reactions of the type

$$\tfrac{1}{2}[\bar{1}\,0\,1] + \tfrac{1}{2}[0\,1\,\bar{1}] \rightarrow \tfrac{1}{2}[\bar{1}\,1\,0] \qquad (5)$$

Similar networks were observed by Lewis [7] in non-stoichiometric spinel; however, in his case, the networks were part of a larger-scale cell structure with misorientations across the cell boundaries. (A cell structure was also found by Doukhan *et al.* in creep specimens [9].) In the present case, the networks have a smaller scale, resulting in a more uniform dislocation substructure.

The high initial work-hardening rate ($\sim \mu/70$) of stoichiometric spinel deformed at temperatures around 1800° C can be correlated with the observed dislocation substructure. Not only are primary and cross-slip lines observed but all six $\frac{1}{2}\langle 1\,1\,0\rangle$ Burgers vector dislocations are seen, indicating that much

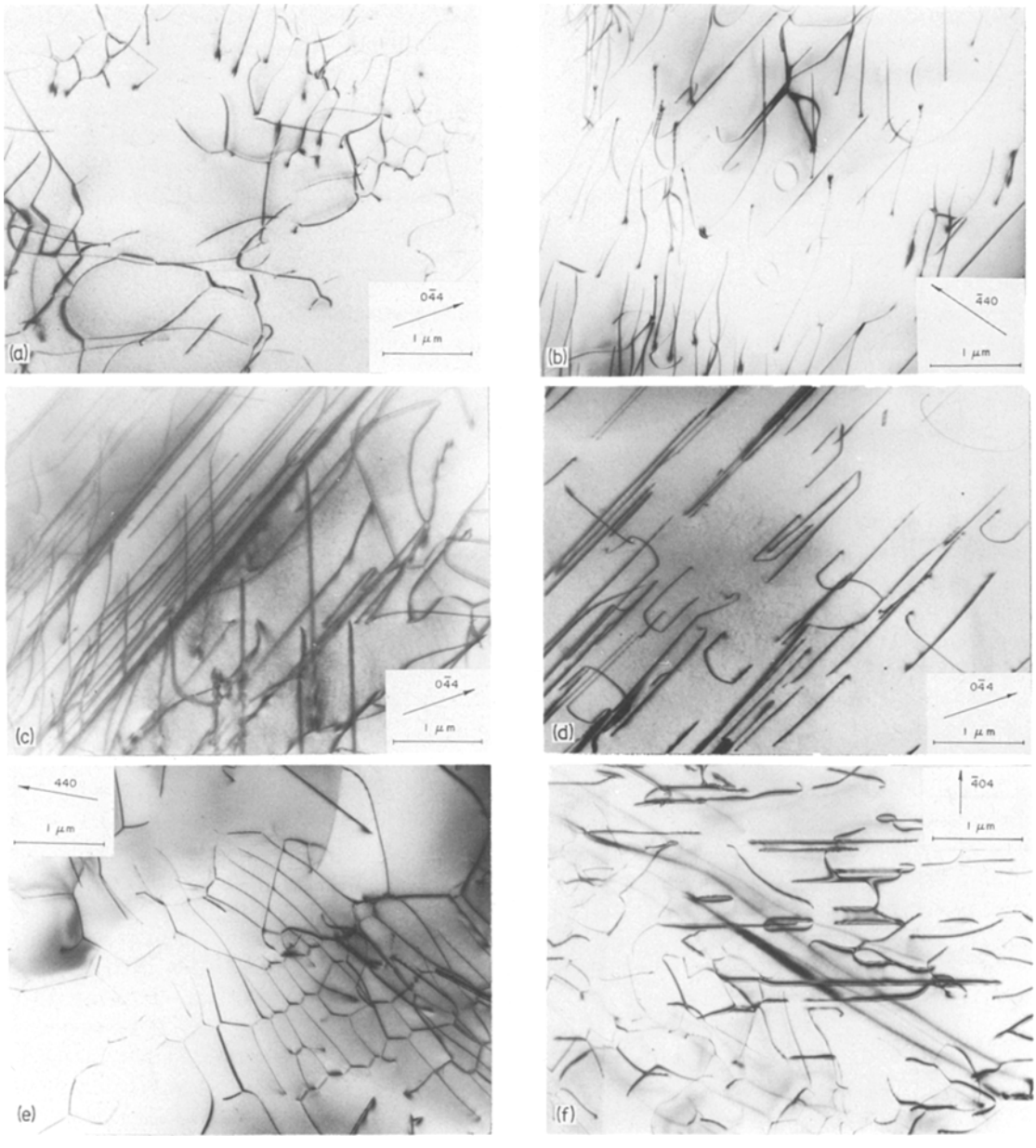

Figure 3 Bright-field transmission electron micrographs of spinel deformed at ~ 1800° C. Operating voltage = 650 kV. **g** vectors are indicated on each micrograph. (a) to (d) Micrographs from one (1 1 1) primary slip plane section, (a) shows a dislocation network section, (b) shows curved dislocations and loops, (c) shows long parallel edge dislocations in a slip band, and (d) shows inclined secondary dislocation, many in the form of dipoles and loops. (e) A (1 1 1) cross-slip plane section showing a hexagonal dislocation network made up of three $\frac{1}{2}\langle 1\,1\,0\rangle$ Burgers vector dislocations. (f) A (1 0 1) section showing a mixture of long edge dislocations, network formation and inclined dipoles and loops. The variety of dislocation images is due to the fact that, for $\mathbf{g} = \bar{4}\,0\,4$, dislocations with different $\frac{1}{2}\langle 1\,1\,0\rangle$ Burgers vectors can give $\mathbf{g}\cdot\boldsymbol{b} = 0$, 2 or 4.

local secondary slip occurred. In addition, the dislocation networks formed by climb are randomly oriented and are, therefore, effective obstacles to glide. The combination of secondary slip and network formation is thought to be responsible for the high work-hardening rates.

The decrease in work-hardening with increasing temperature can also be explained in terms of climb; at the higher temperatures, the climb rate must be sufficiently rapid that annihilation can take place and prevent the rapid build-up in dislocation density.

3. Discussion

3.1. Electrostatic aspects of slip

In order to understand fully the nature of slip in spinel, both the high Peierls stress in stoichiometric crystals and the change from {1 1 1} to {1 1 0} slip and the loss in strength as n increases (Fig. 2) must be explained. A start on these questions was given in the earlier work [2]. The arguments given there will be briefly reiterated, after which other considerations pertinent to {1 1 1} and {1 1 0} slip will be presented.

The stacking order in ⟨1 1 1⟩ directions has been described previously [1, 2]. Oxygen anions are in approximately f c c close-packing, ...abcabc.... Cations are interspersed between the anion layers in two ways: (a) "kagomé" layers in which three-quarters of the octahedral sites are occupied by cations and (b) mixed layers, in which one-quarter of the octahedral and tetrahedral sites are occupied. The stacking can then be written as ...aγbα′cβaγ′-bαcβ′.... where α, β, γ represent the kagomé cation layers and α', β', γ' represent the mixed cation layers. It is likely that glide will occur preferentially within the simpler kagomé layers.

For discussing the Peierls barrier, it is sufficient to consider an $a_0/4$⟨1 1 0⟩ dislocation when it is in the half-slipped position. This is equivalent to considering the translation of cation 1 by $a_0/4$⟨1 1 0⟩ to site 2 (an octahedral position), as shown in the (1 1 1) projection of Fig. 4. As can be seen, two paths are possible althrough the site marked 3,

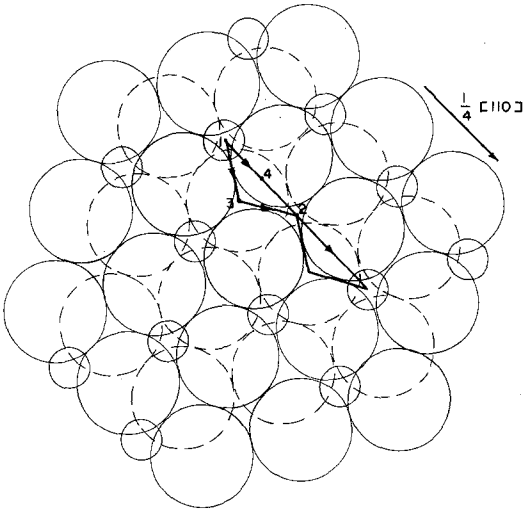

Figure 4 Kagomé layer of spinel projected onto the (1 1 1) plane. The large circles (continuous and dashed) represent oxygen anions in the bottom and top layers respectively, with the smaller circles representing octahedral cations in between these two layers.

which corresponds to Hornstra's synchroshear mechanism, or directly via the path through position 4. In neither case does any severe electrostatic repulsion arise. While the dislocation dissociation corresponding to Equation 2 is implied if the path through site 3 is taken, we have suggested [2], following Doukhan and Escaig [10], that Equation 2 actually describes the core structure of the dislocation. The Peierls barrier in this view is then associated with the maximum energy associated with the path through position 3 in Fig. 4 and should, from electrostatic considerations, vary only slightly with n. (One quarter of the sites on this plane are vacant for $n = 1$; we earlier estimated [2] that an additional 10% of the sites would be vacant at $n = 3.5$.)

The comparable situation for {1 1 0} slip is shown in Fig. 5a and b, projections of the spinel lattice onto a (0 0 1) plane. (Note that the {1 1 0} planes are viewed from the side). Fig. 5a shows the perfect lattice, while Fig. 5b shows the atomic arrangement in the half-slipped position due to passage of a half-partial dislocation, i.e. after a displacement of $a_0/8$ [1 1 0]. (As has been emphasized earlier [2], since dislocation via Equation 1 occurs in all spinels regardless of composition, focus on $a_0/4$⟨1 1 0⟩ dislocations is appropriate when considering the atomistics of slip in spinel.) As will be discussed in detail below, when one consider both anions and cations, {1 1 0} is the closest packed plane in spinel and hence is expected on elementary dislocation theory to be the slip plane. As seen in Fig. 5b, however, an $a_0/4$⟨1 1 0⟩ dislocation will bring tetrahedral and octahedral ions close together in the half slipped position (see, for example, the octahedral ion A and the tetrahedral ion at the 5/8 position in Fig. 5). Furthermore, at the fully slipped position of the half-partial dislocation, some octahedra and tetrahedra share faces across the glide plane. These two factors suggest that there will be a large electrostatic repulsion term in the Peierls barrier for {1 1 0} slip. The net result is that the Peierls barrier is lower for {1 1 1} slip at the stoichiometric composition. As n increases, however, {1 1 0} slip should get easier whenever the dislocation encounters an octahedral vacancy (at a composition of $n = 3.5$, 13.5% of the normally-occupied octahedral sites will be vacant [2]). Recent work in our laboratory [13] concerned with slip bands associated with room-temperature micro-hardness indents in stoichiometric and non-stoichiometric spinel showed that only {1 1 1} slip

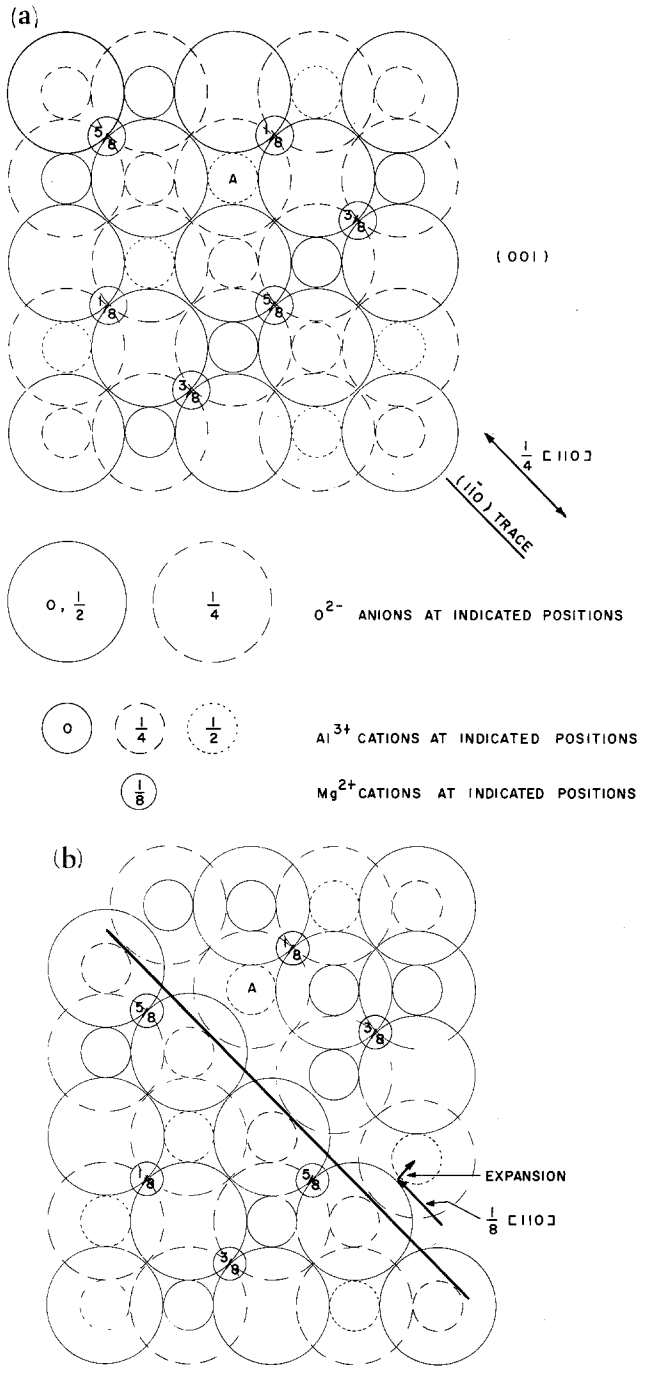

Figure 5 Part of the unit cell of spinel projected onto the (0 0 1) plane. The tetrahedral cations are at the heights indicated. (a) Configuration before glide. (b) Configuration after glide on a (1 $\bar{1}$ 0) plane (shown by a heavy line) by a vector $\frac{1}{8}$ [1 1 0].

occurred; this was true for all compositions although the stoichiometric crystals were the harder, consistent with the high temperature behaviour. This would suggest that {1 1 0} slip is restricted to high temperatures because vacancy diffusion is needed to reduce the Peierls barrier, i.e. a vacancy must diffuse to the position marked A in Fig. 5 for an $a_0/4\langle 1\,1\,0\rangle$ dislocation to move on a {1 1 0} plane.

However, there are geometric aspects which must be considered in addition to the electrostatic aspects just discussed. Consider {1 1 0} slip first.

3.2. Slip on {1 1 0} planes

The stacking of oxygen anions in ⟨1 1 0⟩ directions can be described as a two layer sequence ...abab... . However, when the cations are included, the stacking becomes a four layer sequence ...aba′b′..., where a, a′ layers are mixed anion and octahedral cation layers and the b, b′ layers are mixed anion and combined octahedral and tetrahedral cation layers; this stacking sequence can be readily discerned in Fig. 5a. The spacing of the two layers is $a_0\sqrt{2}/8 = 0.177a_0$. In order to arrive at the half-slipped position, shown in Fig. 5b, the anion and octahedral cations in contact across the slip plane have to ride up over each other, the cations losing a nearest neighbour during the process. Assuming that the ions are acting as hard spheres and that the spinel structure is idealized, it can be shown that the expansion perpendicular to the slip plane in the position shown in Fig. 5b is $0.414r_a$, where r_a is the anion radius. This expansion is a measure of the elastic part of the energy which has to be overcome in order for a dislocation to move on the {1 1 0} plane.

3.3. Slip on {1 1 1} planes

For {1 1 1} slip, the separation between the anion layers is $a_0\sqrt{3}/6 = 0.289a_0$ and between the anion and the cation kagomé layer is $a_0\sqrt{3}/12 = 0.144a_0$. This is less than the spacing between {1 1 0} planes ($0.177a_0$), so that as already mentioned, the {1 1 0} planes are further apart and more close packed and thus ought to be the preferred slip plane. However, geometric aspects of {1 1 1} glide must also be examined more closely. The particular kagomé layer delineated in Fig. 4 is appropriate for this, although a more detailed analysis is needed than for the electrostatic considerations discussed above.

(a) Consider again the synchro-shear mechanism in Fig. 4. In order for this mechanism to operate, the anion in position 3 must move to position 2 by a vector $a_0/12\,[1\,2\,1]$ so that the cation at position 1 can simultaneously move from position 1 to 3 by a vector of $a_0/12\,[2\,1\,\bar{1}]$. The resulting configuration is shown in Fig. 6a. During this motion, the anion has to move between two anions in the layer below, after a displacement of $a_0/24\,[1\,2\,1]$, which involves an expansion perpendicular to the slip plane of $(\sqrt{3} - 2\sqrt{6}/3)r_a = 0.10r_a$.

(b) If the synchro-shear mechanism cannot operate, cations will have to move from position 1 to 2 via 4 in Fig. 4, i.e. by $a_0/8\,[1\,1\,0]$, resulting in the configuration shown in Fig. 6b. The anion has to move over an octahedral cation and the displacement perpendicular to the slip plane has a maximum value at position 4, given by $(\sqrt{15}/3 - \sqrt{6}/3)r_a = 0.475r_a$.

(c) Instead of moving directly along the line between position 1 and 2, the cation may move along a slightly different direction to that of the anions, as also indicated in Fig. 6b; this enables the anions to stay in contact with the anions in the layer below and with the octahedral cation. There

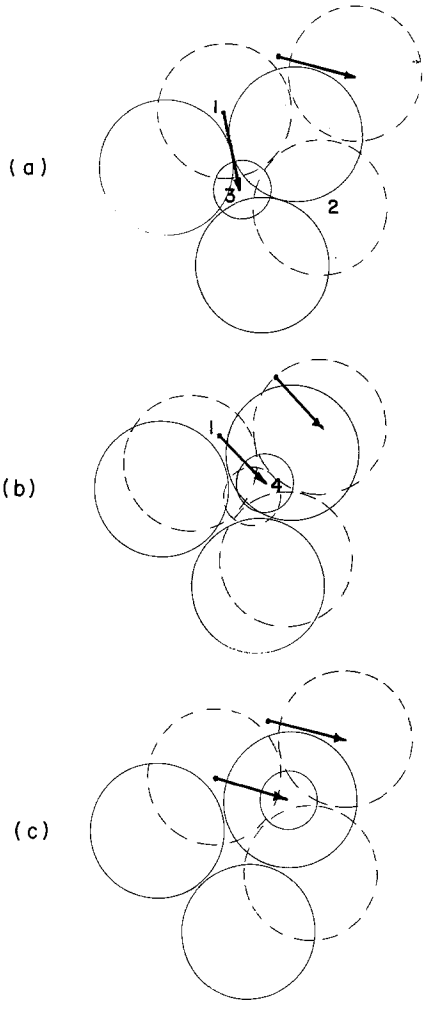

Figure 6 atomic configurations in the kagomé layer of Fig. 4 following glide displacements in various directions. (a) Intermediate stage of the synchro-shear mechanism where the anions have moved $a_0/12\,[1\,2\,1]$ and the cations have moved $a_0/12\,[2\,1\,\bar{1}]$. (b) Configuration after both anions and cations have moved by $a_0/8\,[1\,1\,0]$. The smaller dashed circle indicates an alternate possible position for the cation, as explained for mechanism (c) in the text. (c) Configuration after both anions and cations have moved by $a_0/12\,[1\,2\,1]$.

is a somewhat smaller expansion perpendicular to the slip plane, which can be calculated from Fig. 6b to be $(2\sqrt{3}/3 - \sqrt{6}/3)r_a = 0.338r_a$.

(d) If the anions move by $a_0/12\langle 1\,2\,1\rangle$ vectors carrying the cations with them, the configuration shown in Fig. 6c results. Note that the cations are in tetrahedrally co-ordinated sites. The expansion perpendicular to the slip plane can be calculated to be $(4\sqrt{2}/3 - 2\sqrt{6}/3)r_a = 0.253r_a$.

From the point of view of the displacement perpendicular to the (1 1 1) slip plane, mechanism (b) is the least and mechanism (a) the most likely. To first order, the synchro-shear mechanism will depend on whether the jump frequency of the octahedral cations is high enough to permit Equation 2 to describe the core structure of the dislocation. The necessary jump frequency can be estimated from the dislocation velocity, $v = \dot{\epsilon}/\rho_m b$ where ρ_m is the mobile dislocation density and b the Burgers vector. For $\dot{\epsilon} \sim 10^{-4}\,\text{sec}^{-1}$ and $\rho_m \sim 10^8\,\text{cm}^{-2}$ (Fig. 3), v is $\sim 2 \times 10^{-5}\,\text{cm sec}^{-1}$. This would require a successful cation jump frequency of $\sim 10^3\,\text{sec}^{-1}$. Such jump frequencies are not unreasonable considering the high deformation temperatures and the fact that the cation jumps will be enhanced due to the stress fields associated with the dislocation.

3.4. Stacking fault energy

It is finally necessary to consider the variation of stacking fault energy with composition. As already mentioned, the spacing of the half-partials in spinel has been found to increase with increasing deviation from stoichiometry and the stacking fault energy correspondingly decreases. The data from Welsch *et al.* [8], Lewis [6], and Doukhan and Escaig [10] are summarized in Fig. 7. However, it should be appreicated that the dissociations are on {1 1 1} planes for stoichiometric spinel but on {1 1 0} planes for non-stoichiometric crystals. In both cases, the fault occurs in the cation sublattice while the fcc anion sublattice is undisturbed. While it may be that the stacking fault energy is actually lower on {1 1 1} than on {1 1 0} for stoichiometric spinel but higher than on {1 1 0} for non-stoichiometric spinels, it is not thought that this would cause the change in the observed slip behaviour as n increases. Rabier *et al.* [14] have made calculations for stoichiometric spinel and find that the stacking fault energy is higher on {1 1 1} planes ($1800\,\text{erg cm}^{-2}$) than on {1 1 0} planes ($450\,\text{erg cm}^{-2}$). However, since the former value is much higher than the observed value (Fig. 7), the calculations are suspect. The observed decrease of stacking fault energy on {1 1 0} planes with increasing deviation from stoichiometry is most likely due to the increased number of octahedral cation vacancies; these can probably rearrange themselves near or on the fault plane so as to minimize the electrostatic potential and thus decrease the fault energy.

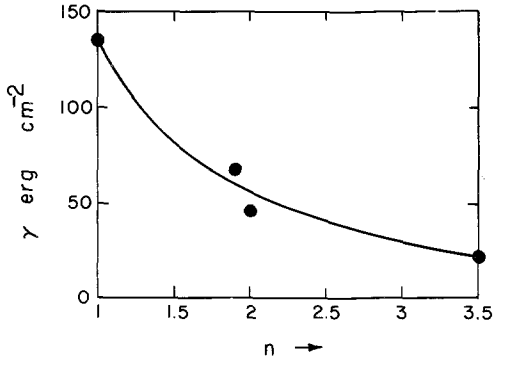

Figure 7 Stacking fault energy, γ, versus n. The data are taken from Welsch *et al.* [8] ($n = 1$), Doukhan and Escaig [10] ($n = 1.8$) and Lewis [6] ($n = 2$ and 3.5).

3.5. {1 1 1} versus {1 1 0} slip

The above discussion shows that the choice between {1 1 1} and {1 1 0} slip planes is not straightforward. {1 1 0} planes are the closest packed planes. However, in analysing the displacement perpendicular to the slip planes during motion, it is apparent that slip on {1 1 1} planes should be easier, whether by the synchro-shear mechanism or by mechanisms (c) or (d) described in Section 3.3. Furthermore, as emphasized previously, {1 1 0} slip in stoichiometric crystals should involve a considerable electrostatic repulsion. Thus, the observation of {1 1 1} glide in stoichiometric spinel is in accord with straightforward aspects of dislocation theory.

In non-stoichiometric spinel, {1 1 0} glide becomes predominant. In addition, the critical resolved shear stress (CRSS) decreases markedly with increasing n (Fig. 2). Lewis [7] found that the CRSS for glide on {1 1 0} planes is a factor of 1.5 smaller than that for glide on {1 1 1} planes in non-stoichiometric spinel. This indicates that glide becomes easier on both {1 1 0} and {1 1 1} planes, but that the Peierls energy decreases more rapidly for {1 1 0} glide with increasing deviation from stoichiometry. As already mentioned, the excess Al_2O_3 is accommodated by cation vacancies on the octahedral sites [6]. The diffusion of these cation

vacancies will lower electrostatic repulsion during {1 1 0} slip [2] and probably also ease the geometric restraints during synchro-shear on {1 1 1} planes. However, examination of Fig. 5a and b reveals that the diffusion of cation vacancies also favours the geometric aspect of {1 1 0} glide. In fact, if the octahedral cations can move fast enough, they will provide no barrier to the movement of the oxygen anions, such that no expansion perpendicular to the {1 1 0} slip plane will be required. It is, therefore, concluded that the preference for {1 1 0} slip in non-stoichiometric spinel at high temperatures can be explained entirely in terms of the diffusion of the excess octahedral vacancies.

Acknowlegement

This research was partly supported by the U.S. Army Research Office under Grant No. AROD 3112473G95. The experimental work was supported by the Office of Naval Research, Grant No. N00014-67-A-040-0003 032-508.

References

1. J. HORNSTRA, *J. Phys. Chem. Solids* **15** (1960) 311.
2. L. HWANG, A. H. HEUER and T. E. MITCHELL, in "Deformation of Ceramic Materials" (Plenum Press, New York, 1975) p. 257.
3. G. E. BACON, *Acta Cryst.* **5** (1952) 684.
4. E. STOLL, P. FISCHER, W. HÄLG and G. MAIER, *J. Physique* **25** (1964) 447.
5. F. BERTAUT, *J. de Phys. Rad.* **12** (1951) 252.
6. H. JAGODINSKI and H. SAALFIELD, *Z. Krist.* **110** (1958) 197.
7. M. H. LEWIS, *Phil. Mag.* **17** (1968) 481.
8. G. WELSH, L. HWANG, A. H. HEUER and T. E. MITCHELL, *ibid.* **29** (1974) 1371.
9. N. DOUKHAN, R. DUCLOS and B. ESCAIG, *J. Physique* **34** (1973) C9-379.
10. N. DOUKHAN, and B. ESCAIG, *ibid.* **35** (1974) L-181.
11. K. C. RADFORD and C. W. A. NEWEY, *Proc. Brit. Ceram. Soc.* 9 (1967) 131.
12. K. ANDO and Y. OISHI, *J. Chem. Phys.* **61** (1974) 625.
13. W. D. BRENTNALL, T. E. MITCHELL and A. H. HEUER, to be published.
14. J. RABIER, P. VEYSSIÉRE and J. GRILHÉ, *J. Physique* **34** (1973) C9-373.

Received 16 June and accepted 16 July 1975.